

Riding the Wave: Polymers in Time-dependent Nonequilibrium Baths

Bhavesh Valecha^{1,*}, Jens-Uwe Sommer^{2,3,†} and Abhinav Sharma^{1,2,‡}

¹*Mathematisch-Naturwissenschaftlich-Technische Fakultät, Institut für Physik,
Universität Augsburg, Universitätsstraße 1, 86159 Augsburg, Germany*

²*Leibniz-Institut für Polymerforschung Dresden, Institut Theorie der Polymere, 01069 Dresden, Germany*

³*Technische Universität Dresden, Institut für Theoretische Physik, 01069 Dresden, Germany*

(Dated: March 4, 2026)

Directed transport is a characteristic feature of numerous biological systems in response to signals such as nutrient and chemical gradients. These signals often depend on time owing to the high complexity of interactions in these systems. In this study, we focus on the steady-state behavior of polymeric systems responding to such time-dependent signals. We model them as ideal Rouse polymers submerged in a nonequilibrium bath, which is described by a spatially and temporally varying self-propulsion wave field. Through a coarse-graining analysis, we show that these polymers display rich emergent response to the temporal stimuli as a function of their length and topology. In particular, long polymers and structures with ring and star topologies *ride the wave*, displaying a positive drift in the direction of the wave. Whereas, shorter polymers and fully connected structures drift against the wave signal. We confirm these analytical predictions with robust numerical simulations, showing that the response of polymeric systems to temporal stimuli can be controlled by the topology or the length of the polymer.

I. INTRODUCTION

Living systems across all scales are characterized by the conversion of stored or ambient energy for various purposes like maintenance of biological processes or to perform systematic movement. These systems are inherently out of equilibrium and have been collectively termed as *active matter*[1–4]. A ubiquitous class of active systems in biology are polymeric molecules which exhibit directed motion and transport, crucial to many cellular processes[5]. Examples are DNA and RNA transcription inside the nucleus[6], ATP-dependent dynamics of chromosomal loci[7] and chromatin[8] during interphase stage of the cell, and molecular motors determining the structure and conformation of the cellular cytoskeletal network[9, 10]. Moreover, many bacteria exist as elongated[11] or chain-like[12] forms and show very rich collective behavior. Mimicking these features in synthetic systems is naturally desirable with applications ranging from drug delivery[13–15], environmental cleanup[16, 17] to cargo transport[18–20]. While this has been achieved in synthetic active systems using external feedback mechanisms[21–23], it might not be always possible to externally monitor and tune the state of the system.

There have been multiple analytical studies exploring directed motion as an emergent phenomenon in model systems of active particles. In spatially varying activity fields, systems such as chiral and achiral active particle connected to a passive load[24, 25], two active particles connected in a dumbbell configuration with fixed orientations[26], and a chiral active dimer[27] can show

accumulation in regions of high activity. These studies have also been extended to include polymeric systems made with active particles that show preferential accumulation depending on the polymer length[28, 29]. However, treatment of such systems in the more general scenario of temporally and spatially varying activity fields has been limited to single active particles[30–32] or an active-passive dimer[33].

Motivated to fill this gap, we consider active Rouse polymers in contact with a nonequilibrium bath, which appears as a spatially and temporally varying activity wave field experienced by the individual monomers. We show analytically that these polymers show directed transport in response to the activity waves, characterized by a systematic drift. Specifically, long polymer chains display a drift along the wave propagation localizing at the wave crests, whereas short chains drift against the wave. Furthermore, the polymer architecture also affects the response to a traveling wave, with the star topology outperforming other architectures with same number of monomers.

II. THE MODEL & RESULTS

We consider an active Rouse polymers immersed in a thermal bath at temperature T in d -spatial dimensions, composed of N monomer units interacting via the quadratic Hamiltonian

$$\mathcal{H} = \frac{\kappa}{2} \sum_{i,j=0}^{N-1} M_{ij} \mathbf{X}_i \cdot \mathbf{X}_j, \quad (1)$$

where \mathbf{X}_i is the position of the i -th monomer and κ is the strength of the harmonic interaction. M_{ij} is the connectivity matrix and it determines the polymer topology[34]. Neglecting inertial dynamics, we model the monomers

* bhavesh.valecha@uni-a.de

† jens-uwe.sommer@tu-dresden.de

‡ abhinav.sharma@uni-a.de

as active Ornstein-Uhlenbeck particles (AOUPs)[35–37], described by the following set of N coupled overdamped Langevin equations

$$\dot{\mathbf{X}}_i = -\mu \nabla_{\mathbf{X}_i} \mathcal{H} + v_a(\mathbf{X}_i - \mathbf{v}_w t) \boldsymbol{\eta}_i + \sqrt{2D} \boldsymbol{\xi}_i. \quad (2)$$

Here, μ represents the monomer mobility, and $\{\boldsymbol{\xi}_i\}$ are N independent zero mean white Gaussian noises, characterized by the correlations $\langle \boldsymbol{\xi}_i(t) \otimes \boldsymbol{\xi}_j(t') \rangle = \delta_{ij} \mathbb{1} \delta(t - t')$ with \otimes denoting the outer product. D is the individual monomer diffusivity which relates to the mobility μ and the temperature T via the Einstein relation $D = \mu T$, with the Boltzmann constant set to unity $k_B = 1$. Each monomer also experiences a spatially and temporally inhomogeneous self-propulsion wave field $v_a(\mathbf{X} - \mathbf{v}_w t)$ moving with a constant speed of v_w in the direction $\hat{\mathbf{e}}_w$, as shown in Fig.1. This field will henceforth be referred to as the activity field. The functional dependence of the traveling wave on the spatial coordinate has been left general. The self-propulsion on monomer i acts along the orientation vector $\boldsymbol{\eta}_i$, which evolves as an Ornstein-Uhlenbeck process in d dimensions, with correlation time τ and variance d^{-1} ,

$$\dot{\boldsymbol{\eta}}_i = -\tau^{-1} \boldsymbol{\eta}_i + \sqrt{2(\tau d)^{-1}} \boldsymbol{\zeta}_i. \quad (3)$$

$\{\boldsymbol{\zeta}_i\}$ are independent zero mean white Gaussian noises with correlations $\langle \boldsymbol{\zeta}_i(t) \otimes \boldsymbol{\zeta}_j(t') \rangle = \delta_{ij} \mathbb{1} \delta(t - t')$. This implies that the orientation vectors also have zero mean and are exponentially correlated $\langle \boldsymbol{\eta}_i(t) \otimes \boldsymbol{\eta}_i(t') \rangle = d^{-1} \mathbb{1} \exp(|t - t'|/\tau)$. The variance has been chosen such that the orientation vectors have the property of unit average modulus $\langle \|\boldsymbol{\eta}_i^2\| \rangle = 1$ for any dimension d .

As is usually done while analysing Rouse polymers, we perform a coordinate transformation to the Rouse domain[38] as: $\boldsymbol{\chi}_i = \sum_j \varphi_{ij} \mathbf{X}_j$. Here, φ_{ij} is the matrix that orthogonally diagonalizes the connectivity matrix M_{ij} , and with its rows normalized to unity. We further transform to the co-moving frame of the zeroth Rouse mode, i.e., $\boldsymbol{\chi}_0 \rightarrow \boldsymbol{\chi}_0 - N \mathbf{v}_w t$. The equations of motion for the Rouse modes are then given by

$$\begin{aligned} \dot{\boldsymbol{\chi}}_0 &= -N \mathbf{v}_w - \gamma_0 \boldsymbol{\chi}_0 + \sum_{j=0}^{N-1} \varphi_{ij} v_a(\mathbf{X}_j - \mathbf{v}_w t) \boldsymbol{\eta}_j + \sqrt{2D} \boldsymbol{\xi}'_0, \\ \dot{\boldsymbol{\chi}}_i &= -\gamma_i \boldsymbol{\chi}_i + \sum_{j=0}^{N-1} \varphi_{ij} v_a(\mathbf{X}_j - \mathbf{v}_w t) \boldsymbol{\eta}_j + \sqrt{2D} \boldsymbol{\xi}'_i, \quad i \geq 1 \end{aligned} \quad (4)$$

where, $\tau_0 = 1/\mu\kappa$ is the monomer relaxation time and $\gamma_i = \mu\kappa\lambda_i$ are the inverse relaxation timescales of the Rouse modes in the absence of activity, which are determined by the eigenvalues $\{\lambda_i\}$ of the connectivity matrix M_{ij} . The noises $\{\boldsymbol{\xi}'_i\}$ are also independent white Gaussian noises with the same statistics as $\{\boldsymbol{\xi}_i\}$. It is important to point out that the presence of the activity term $\sum_{j=0}^{N-1} \varphi_{ij} v_a(\mathbf{X}_j - \mathbf{v}_w t) \boldsymbol{\eta}_j$ couples all the Rouse modes, unlike the case of a passive Rouse polymer in equilibrium. A few comments about the Rouse modes and the

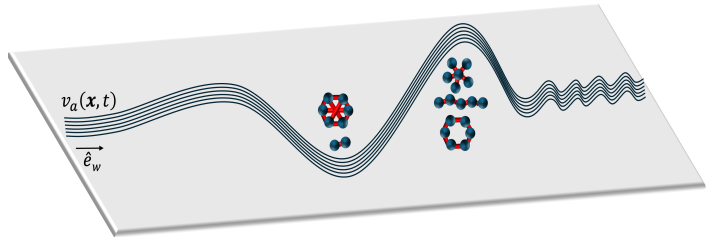


FIG. 1. Schematic of active polymers of varying lengths and connectivity experiencing an activity signal, varying in space and time. The signal is represented as a traveling wave $v_a(\mathbf{x}, t)$ propagating along $\hat{\mathbf{e}}_w$. Polymers with a higher degree of polymerization and low connectivity follow the wave peaks and drift in the wave direction, whereas, shorter polymers and fully connected structures follow the wave valleys and drift against the wave.

choice of coordinate transformations are in order here. $\boldsymbol{\chi}_0$ is related to the center of mass of the polymer by $\mathbf{X}_{\text{COM}} = \boldsymbol{\chi}_0 / \sqrt{N}$, where the \sqrt{N} factor comes from the normalization of the matrix φ_{ij} to have unit normalized rows. Furthermore, this results in the diffusivities of all Rouse modes to scale with a factor N , hence the transformation to the co-moving frame of the zeroth Rouse mode with the same factor.

Since the equations of motion governing the Rouse modes and the orientation vectors are Markovian, the joint probability density $\mathcal{P}(\{\boldsymbol{\chi}\}, \{\boldsymbol{\eta}\}, t)$ evolves according to the Fokker-Planck equation (FPE)[39]

$$\partial_t \mathcal{P} = (\mathcal{L}_0 + \mathcal{L}_\eta + \mathcal{L}_a) \mathcal{P}, \quad (5)$$

where the operators \mathcal{L}_0 , \mathcal{L}_η and \mathcal{L}_a give rise to the free diffusion, orientation and activity dynamics respectively, and are given by

$$\begin{aligned} \mathcal{L}_0 &= \sum_{i=0}^{N-1} \nabla_i \cdot [\gamma_i \boldsymbol{\chi}_i + D \nabla_i] + N \nabla_0 \cdot \mathbf{v}_w, \\ \mathcal{L}_\eta &= (d\tau)^{-1} \sum_{i=0}^{N-1} \tilde{\nabla}_i \cdot [d\boldsymbol{\eta}_i + \tilde{\nabla}_i], \\ \mathcal{L}_a &= \sum_{i=0}^{N-1} \nabla_i \cdot \left[- \sum_{j=0}^{N-1} \varphi_{ij} v_a(\mathbf{X}_j - \mathbf{v}_w t) \boldsymbol{\eta}_j \right], \end{aligned} \quad (6)$$

where we have used the short-hand notation $\nabla_i \equiv \nabla_{\boldsymbol{\chi}_i}$ and $\tilde{\nabla}_i \equiv \nabla_{\boldsymbol{\eta}_i}$.

We are interested in the transport properties of the active polymers in the presence of a traveling activity signal. To this end, we attempt a coarse-grained

description at the level of the center of mass of the polymer $\mathbf{X}_{\text{COM}} = \boldsymbol{\chi}_0/\sqrt{N}$, similar to the analyses in [25, 28, 33, 40]. This is done via a moment-expansion of the joint probability density $\mathcal{P}(\{\boldsymbol{\chi}\}, \{\boldsymbol{\eta}\}, t)$ in the eigenfunctions of the operator \mathcal{L}_η . Following this, we project the FPE Eq. (5) onto the respective eigenfunctions to obtain time-evolution equations for physically relevant fields like the position density, average orientation, etc. In particular, the marginalized position probability density, $\rho_0(\boldsymbol{\chi}_0, t) \equiv \int d\boldsymbol{\eta} \int_{h \neq 0} d\boldsymbol{\chi}_h \mathcal{P}(\{\boldsymbol{\chi}\}, \{\boldsymbol{\eta}\}, t)$ evolves as

$$\partial_t \rho_0 = -\nabla_0 \cdot \left[-N\mathbf{v}_w \rho_0 - D\nabla_0 \rho_0 + \sum_{j=0}^{N-1} \varphi_{0j} \int_{h \neq 0} d\boldsymbol{\chi}_h v_a(\mathbf{X}_j - \mathbf{v}_w t) \boldsymbol{\sigma}_j \right], \quad (7)$$

where, $\boldsymbol{\sigma}_j(\{\boldsymbol{\chi}\}, t) \equiv \int d\boldsymbol{\eta} \boldsymbol{\eta}_j \mathcal{P}(\{\boldsymbol{\chi}\}, \{\boldsymbol{\eta}\}, t)$ is the conditional average orientation of the j -th monomer, given that the polymer configuration is $\{\boldsymbol{\chi}\}$. The $\boldsymbol{\sigma}_j(\{\boldsymbol{\chi}\}, t)$ dynamics are given by

$$\begin{aligned} \partial_t \boldsymbol{\sigma}_j = & -\frac{1}{\tau} \boldsymbol{\sigma}_j + N\nabla_0 \cdot \mathbf{v}_w \boldsymbol{\sigma}_j + \sum_{k=0}^{N-1} \nabla_k \cdot [\gamma_k \boldsymbol{\chi}_k + D\nabla_k] \boldsymbol{\sigma}_j \\ & - \sum_{k=0}^{N-1} \nabla_k \cdot \left[\frac{\varphi_{kj}}{d} v_a(\mathbf{X}_j - \mathbf{v}_w t) \boldsymbol{\varrho} \right] + \mathcal{O}(\nabla^2), \end{aligned} \quad (8)$$

where $\boldsymbol{\varrho}$ is the joint position probability density $\boldsymbol{\varrho} \equiv \int d\boldsymbol{\eta} \mathcal{P}(\{\boldsymbol{\chi}\}, \{\boldsymbol{\eta}\}, t)$, and we have incorporated the dependencies on higher order conditional moments in $\mathcal{O}(\nabla^2)$. Interestingly, we find an equivalence with the active Brownian polymer model [28, 29] by substituting $\tau^{-1} = (d-1)D_r$, where the self-propulsion of the active monomers is modeled as rotational Brownian processes with diffusion coefficient D_r . Thus, our coarse-grained analysis holds independently for the model of activity.

For an analytical treatment of the hierarchy of evolution equations obtained from the moment expansion, we employ the *small gradients* approximation and the *adiabatic* approximation. That is, we assume that the gradients in activity ∇v_a are small compared to the persistence length $l_p = v_a \tau$, as well as, the typical bond length of the polymer $l_b = \sqrt{dT/\kappa}$. This allows us to truncate the expansions in equations of motion Eq. (7) and Eq. (8) by neglecting dependencies on higher order gradients. We further point out that the marginalized density $\rho_0(\boldsymbol{\chi}_0, t)$ is the only slow variable in our description as it satisfies a continuity equation $\partial_t \rho_0(\boldsymbol{\chi}_0, t) = -\nabla_0 \cdot \mathcal{J}(\boldsymbol{\chi}_0, t)$. And, $\{\boldsymbol{\sigma}_j\}$ and all higher order conditional moments are fast variables, characterized by the presence of sink terms, like $-\tau^{-1} \boldsymbol{\sigma}_j$, in their time evolution. Thus, the fast variables are *quasi-static* at timescales at which the slow variable $\rho_0(\boldsymbol{\chi}_0, t)$ evolves. Together, these approximations allow us to close the infinite hierarchy of evolution equations

at the level of $\rho_0(\boldsymbol{\chi}_0, t)$ and $\{\boldsymbol{\sigma}_j\}$. In particular, we obtain a local drift-diffusion equation for the marginalized position probability density $\rho_0(\boldsymbol{\chi}_0, t)$

$$\partial_t \rho_0 = \nabla_0 \cdot [\mathcal{V}_{\text{eff}} - \nabla_0 (\mathcal{D}_{\text{eff}} \rho_0)], \quad (9)$$

where, we have introduced the effective drift $\mathcal{V}_{\text{eff}}(\boldsymbol{\chi}_0)$ and effective diffusivity $\mathcal{D}_{\text{eff}}(\boldsymbol{\chi}_0)$ given by

$$\begin{aligned} \mathcal{V}_{\text{eff}}(\boldsymbol{\chi}_0) &= \left(1 - \frac{\epsilon}{2}\right) \frac{\tau}{d} \nabla_0 v_a^2 \left(\frac{\boldsymbol{\chi}_0}{\sqrt{N}}\right) - N\mathbf{v}_w, \\ \mathcal{D}_{\text{eff}}(\boldsymbol{\chi}_0) &= D + \frac{\tau}{d} v_a^2 \left(\frac{\boldsymbol{\chi}_0}{\sqrt{N}}\right). \end{aligned} \quad (10)$$

The details of this coarse-graining procedure and the approximations can be found in the appendices.

Above equations reveal that the effective diffusivity of the center of mass is enhanced by the presence of activity. And, the effective drift is proportional to the gradient of effective diffusivity through the *tactic response parameter* ϵ . This parameter depends on the polymer properties, length and topology, through the persistence time τ of the active forces and the inverse relaxation times $\{\gamma_i\}$ of the Rouse modes, and is given by

$$\epsilon = 1 - \sum_{i=1}^{N-1} \frac{1}{1 + \tau \gamma_i}. \quad (11)$$

Eq. (10) and Eq. (11) constitute the central results of this work. Particularly, the parameter ϵ dictates the response of the active polymer to the time-varying activity signal. For $\epsilon < 0$, polymer tends to localize in the traveling wave maxima, while for $\epsilon > 0$, the polymer accumulates in the wave minima. This is captured by the steady-state density profile, which can be derived by considering a co-moving box of length L with periodic boundary conditions (see Appendix C)

$$\rho_0(\boldsymbol{\chi}_0) = \frac{\mathcal{D}_{\text{eff}}^{-1}(\boldsymbol{\chi}_0) \int_0^L dx \exp\left\{ \left\{ - \int_{\boldsymbol{\chi}_0}^{\boldsymbol{\chi}_0+x} dy \frac{\mathcal{V}_{\text{eff}}(y)}{\mathcal{D}_{\text{eff}}(y)} \right\} \right\}}{\int_0^L du \int_0^L dx \mathcal{D}_{\text{eff}}^{-1}(u) \exp\left\{ \left\{ - \int_u^{u+x} dy \frac{\mathcal{V}_{\text{eff}}(y)}{\mathcal{D}_{\text{eff}}(y)} \right\} \right\}}. \quad (12)$$

We now show the effect of the polymer length and topology on the steady state accumulation of the polymer in a temporally and spatially inhomogeneous activity field. We assume that the activity field varies sinusoidally in space only along the direction \hat{e}_w with wavelength λ ,

$$v_a(\chi) = v_0 (1 + \sin(\chi/\lambda)). \quad (13)$$

Although chosen for simplicity, we note that any functional form can be generated as a combination of sinusoidal functions, thus keeping this analysis general.

Fig. 2 and Fig. 3 show the steady-state density profiles for active polymers with different lengths and architecture, respectively. The solid lines are analytical expressions from Eq. (12), which are compared with symbols generated with Langevin dynamics simulations (see Appendix D). These plots corroborate our theoretical prediction that the steady-state density can be influenced by

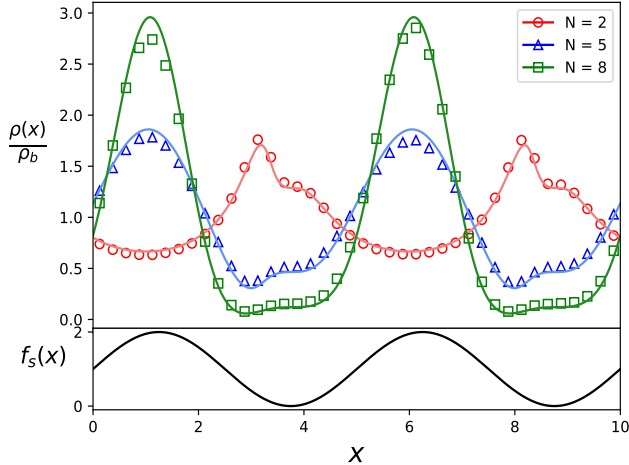


FIG. 2. Steady state density profiles for linear active polymers of different lengths in 2-dimensions. The bottom panel shows the activity field $f_s(x) = v_0[1 + \sin(4\pi x/L)]$ experienced by the active monomers. The y -axis in the top panel is normalized with the bulk density, defined as $\rho_b = 1/L$, where $L = 10.0$ is the simulation box size with periodic boundary conditions. The parameters of the simulation are $v_w = 10^{-2}$, $k_B T = 10^{-3}$, $k = 5.0$, $\gamma = 1.0$, $D_R = 10.0$, and $v_0 = 1.0$.

two factors: the degree of polymerization and the polymer topology. Specifically, for fixed external parameters τ , κ and μ , short polymers tend to localize in regions of low activity and thus follow the wave troughs, whereas, longer polymers accumulate in high activity regions and follow the wave crests. Furthermore, for a polymer with fixed number of monomers, structures with low average connectivity such as a linear chain, a star and a ring tend to follow the wave crests and accumulate where the activity is high, whereas, a fully connected ‘clique’ structure shows accumulation in low activity regions and follows the wave troughs.

Moreover, this stationary density is in fact a *non-equilibrium steady state* as it features a non-vanishing constant flux J_0 . This is reflected in the average drift acquired by the center of the mass of the polymer in the lab frame along the wave direction \hat{e}_w , which is given by [32, 41, 42]

$$v_d = \sum_{i=0}^{N-1} \frac{\langle \dot{\mathbf{X}}_i \rangle}{N} + v_w, \quad (14)$$

$$= \frac{L \left[1 - \exp \left\{ \left\{ - \int_0^L dy \frac{\mathcal{V}_{\text{eff}}(y)}{\mathcal{D}_{\text{eff}}(y)} \right\} \right\} \right]}{\int_0^L du \int_0^L dx \mathcal{D}_{\text{eff}}^{-1}(u) \exp \left\{ \left\{ - \int_u^{u+x} dy \frac{\mathcal{V}_{\text{eff}}(y)}{\mathcal{D}_{\text{eff}}(y)} \right\} \right\}}.$$

In Fig. 4 and Fig. 5, we report the average drift v_d of the center of mass of polymers with varying degrees of polymerization and connectivity, respectively. These plots and Eq. (14) show that the drift attained by the polymer depends on the polymer properties, i.e., on ϵ through the

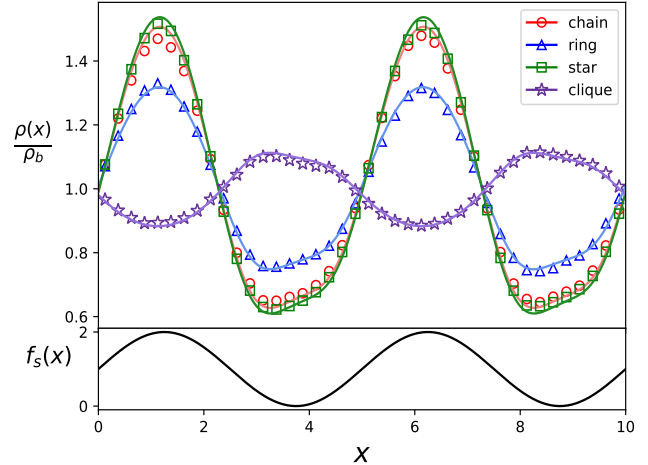


FIG. 3. Steady state density profiles for active polymers of different architecture (topology) in 2-dimensions, each composed of $N = 6$ monomers. The bottom panel shows the activity field $f_s(x) = v_0[1 + \sin(4\pi x/L)]$ experienced by the active particle. The y -axis in the top panel is normalized with the bulk density, defined as $\rho_b = 1/L$, where $L = 10.0$ is the simulation box size with periodic boundary conditions. The parameters of the simulation are $v_w = 10^{-2}$, $k_B T = 10^{-1}$, $k = 5.0$, $\gamma = 1.0$, $D_R = 5.0$, and $v_0 = 1.0$.

ratio: $\mathcal{V}_{\text{eff}}/\mathcal{D}_{\text{eff}}$. Specifically depending on the sign of ϵ , the polymer has a non-trivial response to the traveling wave - for $\epsilon < 0$, the polymer displays a positive drift, $v_d > 0$, in the direction of the traveling wave, while for $\epsilon > 0$, the polymer moves against the wave displaying a negative drift, $v_d < 0$. Thus, longer polymers and polymers in linear, star and ring configurations show positive drift, whereas, shorter polymers and a fully connected configuration show negative drift.

These results can be qualitatively explained as follows. From Eq. (11), we see that the sign of ϵ depends on the contribution of the timescale ratios (τ/τ_i) with $\tau_i = \tau_0/\lambda_i = 1/\gamma_i$ of individual Rouse modes. Modes with relaxation times longer than the correlation time τ of active forces, i.e. $\tau/\tau_i \ll 1$, lead to ϵ being more negative. In fact, when the persistence time is even much smaller than the monomer relaxation time, i.e. for $\tau/\tau_0 \ll 1$ we get $\epsilon \rightarrow 2 - N$, implying that all polymers longer than dimers will follow the traveling wave maxima. For $\tau/\tau_0 > 1$, this threshold is pushed to longer polymers. For linear polymers we have $\lambda_i \simeq i^2/N^2$, so that the longest relaxation time (the Rouse time τ_R) goes as $\tau_R = \tau_1 \simeq N^2$. Comparing this intrinsic relaxation time with the the persistence time τ , we can define a crossover chain length N_c for a given set of parameters τ and τ_0 , scaling as $N_c \simeq (\tau_0/\tau)^{1/2}$. Further, for polymers with different topology, we recall that a fully connected structure (clique) we have only one mode which is given by $\tau_1^{\text{clique}} = N\tau_0$. Thus, such highly compact structures

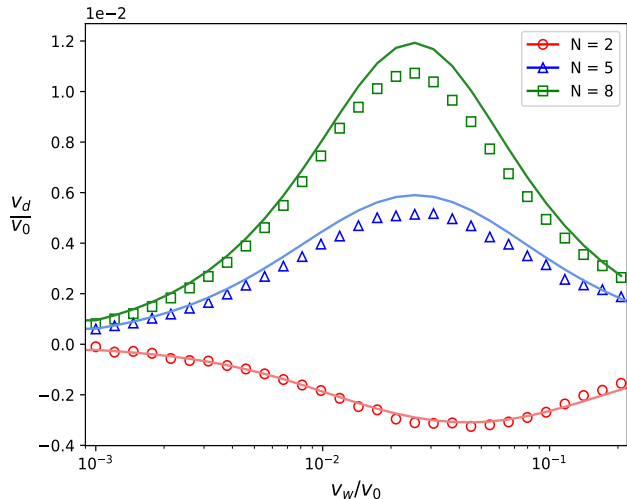


FIG. 4. Average drift for different lengths of the linear active polymers in 2-dimensions. The activity profile is the same as in Fig. 2. Simulation parameters are: $k_B T = 10^{-2}$, $k = 5.0$, $\gamma = 1.0$, $D_R = 10.0$, and $v_0 = 1.0$. The results are obtained by running 10^3 independent trajectories and averaging $(X_{\text{COM}}(t) - X_{\text{COM}}(0))/t$ over these trajectories.

have similar tactic response like a single active particle, which always localizes in low activity regions[43, 44]. We conclude that structures with fewer number of connections between monomers leading to the existence of smaller eigenvalues, λ_1 , usually accumulate in high activity regions, and thus drift along with a traveling activity signal. However, we note that there is no simple relation between ϵ in Eq.(11) and the radius of gyration of a Gaussian connected structure, where the latter is given by $R_g^2 = l^2(1/N) \sum_{k=1}^{N-1} 1/\lambda_k$ where l denotes the Kuhn length of the macromolecule [34].

We reiterate that all the above results hold within the limits of applicability of the the small gradients approximation. This holds for traveling waves with large wavelengths, i.e., $\lambda \gg l_p$, and so when $v_w \ll v_0$. Thus, these theoretical results predict the response of active polymer networks to generic, albeit slow time-dependent activity waves.

III. CONCLUSION & OUTLOOK

Time-dependent stimuli are omnipresent in the biological setting across all scales, from cytoskeletal networks in cells to unicellular bacteria. In this work, we have studied the response of a large class of active systems to such stimuli, namely active polymers in traveling activity waves. Using a simple model, we have shown that these systems display non-trivial transport properties in time-varying activity media. In particular, this response crucially depends on the degree of polymerization and the polymer architecture - longer linear polymers and

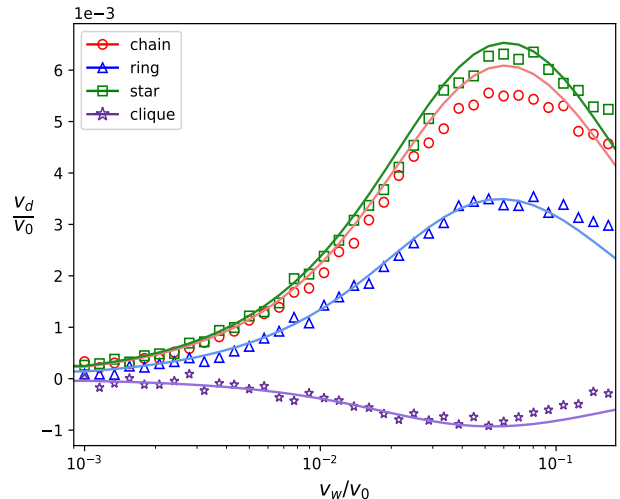


FIG. 5. Average drift for different architectures of the active polymers with $N = 6$ monomers in 2-dimensions. The activity profile is the same as in Fig. 3. Simulation parameters are: $k_B T = 10^{-1}$, $k = 5.0$, $\gamma = 1.0$, $D_R = 5.0$, and $v_0 = 1.0$. The results are obtained by running 10^3 independent trajectories and averaging $(X_{\text{COM}}(t) - X_{\text{COM}}(0))/t$ over these trajectories.

polymers with low average connectivity display a positive drift, accumulating in the wave peaks, in contrast to shorter linear polymers and highly connected polymers, which show a negative drift and accumulate in the wave valleys. This peculiar tactic response can be attributed to the slow Rouse modes of the active polymer that relax on timescales longer than the persistence time of the active forces. These findings extend prior studies of active systems in inhomogeneous activity fields[25, 28, 30, 33, 44] by addressing a previously unexplored regime: active polymer networks subjected to activity landscapes that vary in both space and time. Furthermore, we point out the generality of our approach as it can be easily generalized to consider other interesting systems such as partially active polymer networks[29] and active polymers with different models of activity[28].

Recent advances on the experimental front have made possible engineering synthetic active systems with high precision[45–47]. Prime examples include Janus particles, where the self-propulsion arises from diffusiophoresis by catalytic chemical reactions involving hydrogen peroxide[48], lutidine[49] or hydrazine[50]. Other experimental setups of active colloids also exist, where the self-propulsion is achieved through thermophoresis[51] or electrophoresis[52]. Some of these synthetic active systems can also be assembled into linear chains and other interconnected structures, composed of - millimeter-sized robots[53], magnetic colloidal beads[54, 55], silica-beads with magnetic coating in an electric field[56–58] or diffusiophoretic Janus colloids[59]. These platforms could be excellent testbeds for our theoretical predictions. Furthermore, spatio-temporal signaling networks are crucial

for various intracellular processes[60]. For e.g., temporal dynamics of kinase phosphorylates have been identified to guide the mitotic-spindle self-organization during cell division[60, 61]. This is a relevant biological scenario where our results could be useful.

Finally, we would like to note that our model does not account for the hydrodynamic interactions between the active polymers and the surrounding solvent, a class of models known as dry active matter models [2]. We defer studies investigating this interesting direction to future work.

IV. ACKNOWLEDGEMENTS

A.S. acknowledges support by the Deutsche Forschungsgemeinschaft (DFG) within Project No. SH

1275/5-1. J.U.S. thanks the cluster of excellence “Physics of Life” at TU Dresden for its support. B.V. thanks S. Chebolu for her invaluable support, and F. Faedi and A. Pandit for fruitful discussions.

V. DATA AVAILABILITY

The data that supports these findings is openly available at[62].

-
- [1] S. Ramaswamy, *Annu. Rev. Condens. Matter Phys.* **1**, 323 (2010).
- [2] M. C. Marchetti, J. F. Joanny, S. Ramaswamy, T. B. Liverpool, J. Prost, M. Rao, and R. A. Simha, *Rev. Mod. Phys.* **85**, 1143 (2013).
- [3] S. Ramaswamy, *J. Stat. Mech.* **2017**, 054002 (2017).
- [4] M. t. Vrugt, B. Liebchen, and M. E. Cates, What exactly is ‘active matter’? (2025), arXiv:2507.21621 [cond-mat].
- [5] R. G. Winkler and G. Gompper, *The Journal of Chemical Physics* **153**, 040901 (2020).
- [6] M. Guthold, X. Zhu, C. Rivetti, G. Yang, N. H. Thomson, S. Kasas, H. G. Hansma, B. Smith, P. K. Hansma, and C. Bustamante, *Biophysical Journal* **77**, 2284 (1999).
- [7] S. C. Weber, A. J. Spakowitz, and J. A. Theriot, *Proceedings of the National Academy of Sciences* **109**, 7338 (2012), publisher: Proceedings of the National Academy of Sciences.
- [8] A. Zidovska, D. A. Weitz, and T. J. Mitchison, *Proceedings of the National Academy of Sciences* **110**, 15555 (2013), publisher: Proceedings of the National Academy of Sciences.
- [9] F. C. MacKintosh and A. J. Levine, *Physical Review Letters* **100**, 018104 (2008), publisher: American Physical Society.
- [10] A. Ravichandran, G. A. Vliegenthart, G. Saggiorato, T. Auth, and G. Gompper, *Biophysical Journal* **113**, 1121 (2017), publisher: Elsevier.
- [11] G. K. Auer, P. M. Oliver, M. Rajendram, T.-Y. Lin, Q. Yao, G. J. Jensen, and D. B. Weibel, *mBio* **10**, 10.1128/mbio.00210 (2019), publisher: American Society for Microbiology.
- [12] Y. I. Yaman, E. Demir, R. Vetter, and A. Kocabas, *Nature Communications* **10**, 2285 (2019), publisher: Nature Publishing Group.
- [13] J. Wang and W. Gao, *ACS Nano* **6**, 5745 (2012), publisher: American Chemical Society.
- [14] B. E.-F. de Ávila, P. Angsantikul, J. Li, M. Angel Lopez-Ramirez, D. E. Ramírez-Herrera, S. Thamphiwatana, C. Chen, J. Delezuk, R. Samakapiruk, V. Ramez, M. Obonyo, L. Zhang, and J. Wang, *Nature Communications* **8**, 272 (2017), publisher: Nature Publishing Group.
- [15] M. Mathesh, J. Sun, F. v. d. Sandt, and D. A. Wilson, *Nanoscale* **12**, 22495 (2020), publisher: The Royal Society of Chemistry.
- [16] B. Jurado-Sánchez and J. Wang, *Environmental Science: Nano* **5**, 1530 (2018), publisher: The Royal Society of Chemistry.
- [17] J. Parmar, D. Vilela, K. Villa, J. Wang, and S. Sánchez, *Journal of the American Chemical Society* **140**, 9317 (2018), publisher: American Chemical Society.
- [18] L. Baraban, M. Tasinkevych, M. N. Popescu, S. Sanchez, S. Dietrich, and O. G. Schmidt, *Soft Matter* **8**, 48 (2011), publisher: The Royal Society of Chemistry.
- [19] X. Ma, K. Hahn, and S. Sanchez, *Journal of the American Chemical Society* **137**, 4976 (2015), publisher: American Chemical Society.
- [20] H. Merlitz, C. Wu, and J.-U. Sommer, *Soft Matter* **13**, 3726 (2017), publisher: The Royal Society of Chemistry.
- [21] B. Qian, D. Montiel, A. Bregulla, F. Cichos, and H. Yang, *Chem. Sci.* **4**, 1420 (2013).
- [22] T. Mano, J.-B. Delfau, J. Iwasawa, and M. Sano, *Proc. Natl. Acad. Sci. U.S.A.* **114**, E2580 (2017).
- [23] H. Massana-Cid, D. Levis, R. J. H. Hernández, I. Pagonabarraga, and P. Tierno, *Phys. Rev. Res.* **3**, L042021 (2021).
- [24] B. Valecha, H. Vahid, P. L. Muzzeddu, J.-U. Sommer, and A. Sharma, *Soft Matter* **21**, 3384 (2025), publisher: The Royal Society of Chemistry.
- [25] H. D. Vuijk, H. Merlitz, M. Lang, A. Sharma, and J.-U. Sommer, *Phys. Rev. Lett.* **126**, 208102 (2021).
- [26] H. D. Vuijk, S. Klempahn, H. Merlitz, J.-U. Sommer, and A. Sharma, *Phys. Rev. E* **106**, 014617 (2022).
- [27] P. L. Muzzeddu, H. D. Vuijk, H. Löwen, J.-U. Sommer, and A. Sharma, *J. Chem. Phys.* **157**, 134902 (2022).
- [28] P. L. Muzzeddu, A. Gambassi, J.-U. Sommer, and A. Sharma, *Phys. Rev. Lett.* **133**, 118102 (2024).
- [29] S. Ravichandir, B. Valecha, P. L. Muzzeddu, J.-U. Sommer, and A. Sharma, *Soft Matter* **21**, 1835 (2025), publisher: The Royal Society of Chemistry.
- [30] A. Geiseler, P. Hänggi, F. Marchesoni, C. Mulhern, and S. Savel’ev, *Physical Review E* **94**, 012613 (2016).

- [31] A. Geiseler, P. Hänggi, and F. Marchesoni, *Scientific Reports* **7**, 41884 (2017).
- [32] H. Merlitz, H. D. Vuijk, J. Brader, A. Sharma, and J.-U. Sommer, *J. Chem. Phys.* **148**, 194116 (2018).
- [33] P. L. Muzzeddu, É. Roldán, A. Gambassi, and A. Sharma, *EPL* **142**, 67001 (2023).
- [34] J.-U. Sommer and A. Blumen, *Journal of Physics A: Mathematical and General* **28**, 6669 (1995).
- [35] L. Caprini and U. M. B. Marconi, *Soft Matter* **15**, 2627 (2019).
- [36] D. Martin, J. O’Byrne, M. E. Cates, E. Fodor, C. Nardini, J. Tailleur, and F. van Wijland, *Physical Review E* **103**, 032607 (2021), publisher: American Physical Society.
- [37] L. Caprini, A. R. Sprenger, H. Löwen, and R. Wittmann, *The Journal of Chemical Physics* **156**, 071102 (2022).
- [38] M. Doi, S. F. Edwards, M. Doi, and S. F. Edwards, *The Theory of Polymer Dynamics*, International Series of Monographs on Physics (Oxford University Press, Oxford, New York, 1988).
- [39] H. Risken, *The Fokker-Planck Equation: Methods of Solution and Applications*, edited by H. Haken, Springer Series in Synergetics, Vol. 18 (Springer, Berlin, Heidelberg, 1996).
- [40] M. E. Cates and J. Tailleur, *EPL* **101**, 20010 (2013).
- [41] N. S. Goel, *Stochastic models in biology* (Academic Press, New York, 1974).
- [42] P. Hänggi and F. Marchesoni, *Rev. Mod. Phys.* **81**, 387 (2009).
- [43] M. J. Schnitzer, *Phys. Rev. E* **48**, 2553 (1993).
- [44] A. Sharma and J. M. Brader, *Phys. Rev. E* **96**, 032604 (2017).
- [45] C. Bechinger, R. Di Leonardo, H. Löwen, C. Reichhardt, G. Volpe, and G. Volpe, *Rev. Mod. Phys.* **88**, 045006 (2016).
- [46] H. Löwen, *Europhysics Letters* **121**, 58001 (2018).
- [47] R. Niu and T. Palberg, *Soft Matter* **14**, 7554 (2018).
- [48] J. R. Howse, R. A. L. Jones, A. J. Ryan, T. Gough, R. Vafabakhsh, and R. Golestanian, *Phys. Rev. Lett.* **99**, 048102 (2007).
- [49] I. Buttinoni, *Physical Review Letters* **110**, 10.1103/PhysRevLett.110.238301 (2013).
- [50] W. Gao, A. Pei, R. Dong, and J. Wang, *Journal of the American Chemical Society* **136**, 2276 (2014).
- [51] H.-R. Jiang, *Physical Review Letters* **105**, 10.1103/PhysRevLett.105.268302 (2010).
- [52] A. Würger, *Reports on Progress in Physics* **73**, 126601 (2010).
- [53] C. Scholz, A. Ldov, T. Pöschel, M. Engel, and H. Löwen, *Sci. Adv.* **7**, eabf8998 (2021).
- [54] F. Martinez-Pedrero, A. Cebers, and P. Tierno, *Soft Matter* **12**, 3688 (2016).
- [55] R. Mhanna, Y. Gao, I. Van Tol, E. Springer, N. Wu, and D. W. M. Marr, *Langmuir* **38**, 5730 (2022).
- [56] R. Di Leonardo, *Nature Materials* **15**, 1057 (2016).
- [57] H. R. Vutukuri, B. Bet, R. van Roij, M. Dijkstra, and W. T. S. Huck, *Scientific Reports* **7**, 16758 (2017).
- [58] D. Nishiguchi, J. Iwasawa, H.-R. Jiang, and M. Sano, *New Journal of Physics* **20**, 015002 (2018).
- [59] B. Biswas, R. K. Manna, A. Laskar, P. B. S. Kumar, R. Adhikari, and G. Kumaraswamy, *ACS Nano* **11**, 10025 (2017).
- [60] B. N. Kholodenko, *Nature Reviews Molecular Cell Biology* **7**, 165 (2006).
- [61] M. Caudron, G. Bunt, P. Bastiaens, and E. Karsenti, *Science* **309**, 1373 (2005).
- [62] B. Valecha, bhavesh-valecha/rouse-polymers-in-time-dependent- nonequilibrium-baths: Workflow release (citation) (2026).
- [63] M. Abramowitz and I. A. Stegun, *Handbook of Mathematical Functions: With Formulas, Graphs, and Mathematical Tables* (Courier Corporation, 1965) google-Books-ID: MtU8uP7XMv0C.

Appendix A: Coarse-graining Procedure

Here, we entail the coarse-graining procedure to reach Eq. (7) and Eq. (8), starting from the Fokker-Planck equation Eq. (5). This is done in two steps: first by integrating out the orientation degrees of freedom $\{\boldsymbol{\eta}\}$, followed by integrating out all the Rouse modes except $\boldsymbol{\chi}_0$. The moment expansion of $\mathcal{P}(\{\boldsymbol{\chi}\}, \{\boldsymbol{\eta}\}, t)$ in the eigenfunctions of the operator \mathcal{L}_η is given by

$$\mathcal{P}(\{\boldsymbol{\chi}\}, \{\boldsymbol{\eta}\}, t) = \sum_{\mathbf{n}} \phi_{\mathbf{n}}(\{\boldsymbol{\chi}\}, t) u_{\mathbf{n}}(\{\boldsymbol{\eta}\}). \quad (\text{A1})$$

where $\phi_{\mathbf{n}}(\{\boldsymbol{\eta}\}, t)$ are the expansion modes and $u_{\mathbf{n}}(\{\boldsymbol{\eta}\})$ are given in terms of Hermite polynomials in the probabilist’s convention[63] labeled by $N \times d$ matrix of non-negative integers \mathbf{n}

$$u_{\mathbf{n}}(\{\boldsymbol{\eta}\}) = \frac{\exp\left\{-\frac{d \sum_j \eta_j^2}{2}\right\} \prod_{i=0}^{N-1} \prod_{\alpha=1}^d H_{n_{i\alpha}}(\sqrt{d} \eta_{i\alpha})}{(2\pi/d)^{Nd/2}}. \quad (\text{A2})$$

The corresponding eigenfunctions of \mathcal{L}_η are $\psi_{\mathbf{n}} = \tau^{-1} \sum_{i=0}^{N-1} \sum_{\alpha=1}^d n_{i\alpha}$. For projecting the FPE onto the eigenfunctions $u_{\mathbf{n}}$, we define the auxiliary set of functions $\tilde{u}_{\mathbf{n}}(\{\boldsymbol{\eta}\})$, which are orthogonal to $u_{\mathbf{n}}(\{\boldsymbol{\eta}\})$ as

$$\tilde{u}_{\mathbf{n}}(\{\boldsymbol{\eta}\}) = \prod_{i=0}^{N-1} \prod_{\alpha=1}^d \frac{H_{n_{i\alpha}}(\sqrt{d} \eta_{i\alpha})}{n_{i\alpha}!}, \quad (\text{A3})$$

and the orthogonality relation is: $\int \prod_{i=0}^{N-1} d\boldsymbol{\eta}_i \tilde{u}_{\mathbf{m}} u_{\mathbf{n}} = \delta_{\mathbf{m}, \mathbf{n}}$. Now, using this orthogonal property, we project the FPE onto the eigenfunctions $\tilde{u}_{\mathbf{n}}(\{\boldsymbol{\eta}\})$, and using the properties of the Hermite polynomials, we obtain

$$\begin{aligned} \partial_t \phi_{\mathbf{n}} &= \psi_{\mathbf{n}} \phi_{\mathbf{n}} + \mathcal{L}_0 \phi_{\mathbf{n}} \\ &- \nabla_i \cdot \varphi_{ij} v_a(\mathbf{X}_j - \mathbf{v}_w t) \frac{1}{\sqrt{d}} [\phi_{b_{j\alpha} \mathbf{n}} + (n_{j\alpha} + 1) \phi_{b_{j\alpha}^\dagger \mathbf{n}}], \end{aligned} \quad (\text{A4})$$

where $b_{j\alpha}^\dagger, b_{j\alpha}$ are raising and lowering operators, which increase and decrease the (i, α) -component of \mathbf{n} , respectively. The expansion modes $\phi_{\mathbf{n}}$ are proportional to the conditional moments of the orientation vectors $\{\boldsymbol{\eta}\}$ given that the polymer configuration is $\{\boldsymbol{\chi}\}$ as

$$\begin{aligned} \varrho &\equiv \int d\boldsymbol{\eta} \mathcal{P}(\{\boldsymbol{\chi}\}, \{\boldsymbol{\eta}\}, t) = \phi_{\mathbf{0}}, \\ \sigma_{i\alpha} &\equiv \int d\boldsymbol{\eta} \eta \mathcal{P}(\{\boldsymbol{\chi}\}, \{\boldsymbol{\eta}\}, t) = \frac{1}{\sqrt{d}} \phi_{b_{i\alpha}^\dagger \mathbf{0}}, \end{aligned} \quad (\text{A5})$$

where $\mathbf{0}$ is a $N \times d$ matrix with all elements equal to zero. Now, the time evolution for ϱ and $\sigma_{i\alpha}$ are given by specializing Eq. (A4) to $\mathbf{n} = \mathbf{0}$ and $\mathbf{n} = \mathbf{b}_{i\alpha}^\dagger \mathbf{0}$,

$$\begin{aligned} \partial_t \varrho &= - \sum_{i=1}^{N-1} \nabla_i \cdot \left[-\gamma_i \chi_i \varrho - D \nabla_i \varrho \right] \\ &\quad + \sum_{i,j=0}^{N-1} \varphi_{ij} v(\mathbf{X}_j - \mathbf{v}_w t) \sigma_j + \nabla_0 \cdot [\mathbf{v}_w \varrho], \\ \partial_t \sigma_j &= -\frac{1}{\tau} \sigma_j + N \nabla_0 \cdot \mathbf{v}_w \sigma_j + \sum_{k=0}^{N-1} \nabla_k \cdot [\gamma_k \chi_k + D \nabla_k] \sigma_j \\ &\quad - \sum_{k=0}^{N-1} \nabla_k \cdot \left[\frac{\varphi_{kj}}{d} v_a(\mathbf{X}_j - \mathbf{v}_w t) \varrho \right] + \mathcal{O}(\nabla^2). \end{aligned} \quad (\text{A6})$$

This constitutes our first coarse-graining step, where we have integrated out the orientation degrees of freedom. We follow this by coarse-graining all Rouse modes except χ_0 from the equation of motion for ϱ ,

$$\rho_0(\chi_0, t) \equiv \int_{h \neq 0} d\chi_h \varrho(\{\chi\}, t). \quad (\text{A7})$$

This gives us the equation of motion for the marginalized position probability density (Eq. (7)). Similar relations for higher order conditional moments can be derived, however, we recall that our coarse-grained description is limited to the first conditional moment $\{\sigma_{i\alpha}\}$.

Appendix B: Small Gradients Approximation & Adiabatic Approximation

In this appendix, we provide the detailed application of the approximations used to close the infinite hierarchy of equations of motion obtained above. We recall that ϱ and its corresponding coarse-grained version ρ_0 satisfy a continuity equation and are the slow variables in our description. This is in contrast to $\{\sigma\}$ and subsequent higher order conditional moments ϕ_n , which are characterized by the presence of decay terms proportional to the persistence time τ through their corresponding eigenvalues, i.e., $-\psi_n \phi_n$. This leads to a timescale separation between the slow and the fast modes of our coarse-grained description governed by the correlation time τ of the active forces. Thus, the timescales at which the slow modes evolve, the fast modes have already relaxed to their *quasi-stationary* value, given by

$$\begin{aligned} \sigma_i &\approx \tau \sum_{i=0}^{N-1} \nabla_i \cdot [\gamma_i \chi_i + D \nabla_j] \sigma_j + \tau \nabla_0 \cdot [\mathbf{v}_w \sigma_i] \\ &\quad - \tau \sum_{j=0}^{N-1} \nabla_j \cdot \left[\frac{\varphi_{ji} v_a(\mathbf{X}_i - \mathbf{v}_w t) \varrho}{d} \right] + \mathcal{O}(\nabla^2). \end{aligned} \quad (\text{B1})$$

This is the *adiabatic approximation*. It is important to point out that the validity of this approximation strongly

relies on the persistence time τ of the orientation dynamics. If the persistence time is too long, then there is not enough timescale separation between the slow and fast variables, leading to less accurate predictions using this approximation.

We will now employ the *small gradients approximation* to arrive at the effective drift-diffusion equation Eq. (9). Specifically, we assume that the variations in the activity field are small compared to the persistence length $l_p = v_a \tau$ and the polymer bond length $l_b = \sqrt{dT/\kappa}$. That is, we only retain terms up to drift and diffusion order in the expression for $\rho_0(\chi_0, t)$, or, only terms which are linear in ∇v_a in the flux $\mathcal{J}(\chi_0, t)$. We note that this approximation assumes that ρ_0 and \mathcal{J} have small variations when the center of mass of the polymer is displaced, and is independent of the internal structure, i.e., the gradients of other Rouse coordinates can be large.

Using the adiabatic expression for σ_i in the probability current $\mathcal{J}(\chi_0, t)$, we focus on the contribution coming from the activity term,

$$\begin{aligned} \mathcal{J}_a &\equiv \sum_{j=0}^{N-1} \varphi_{0j} \int_{h \neq 0} d\chi_h v_a(\mathbf{X}_j - \mathbf{v}_w t) \sigma_j, \\ &= \tau \sum_{j=0}^{N-1} \varphi_{0j} \int_{h \neq 0} d\chi_h v_a(\mathbf{X}_j - \mathbf{v}_w t) \left[\nabla_0 \cdot [\mathbf{v}_w \sigma_j] \right. \\ &\quad \left. + \sum_{i=0}^{N-1} \nabla_i \cdot [\gamma_i \chi_i + D \nabla_j] \sigma_j \right. \\ &\quad \left. - \sum_{l=0}^{N-1} \nabla_l \cdot \left[\frac{\varphi_{lj} v_a(\mathbf{X}_j - \mathbf{v}_w t) \varrho}{d} \right] \right] + \mathcal{O}(\nabla^2). \end{aligned} \quad (\text{B2})$$

We will now check the order of gradient in the contribution coming from each term in the above expression. Starting with

$$\begin{aligned} &D\tau \sum_{j=0}^{N-1} \varphi_{0j} \int_{h \neq 0} d\chi_h v_a(\mathbf{X}_j - \mathbf{v}_w t) \sum_{i=0}^{N-1} \nabla_i^2 \sigma_j, \\ &= D\tau \sum_{j=0}^{N-1} \varphi_{0j} \int_{h \neq 0} d\chi_h v_a(\mathbf{X}_j - \mathbf{v}_w t) [\nabla_0^2 \sigma_j \\ &\quad + \sigma_j \sum_{i \neq 0} \nabla_i^2 v_a(\mathbf{X}_j - \mathbf{v}_w t)], \\ &= \mathcal{O}(\nabla_0^2), \end{aligned} \quad (\text{B3})$$

where, we have used integration by parts from the first to the second step and converted ∇_i^2 to ∇_0^2 using

$$\begin{aligned} \nabla_j v_a(\mathbf{X}_i) &= \partial_{j\beta} v_a \left(\sum_k \varphi_{ki} \chi_{k\alpha} \right) = \frac{\varphi_{ji}}{\varphi_{j0}} \partial_{0\beta} v_a(\mathbf{X}_i) \\ &= \sqrt{N} \varphi_{ji} \partial_{0\beta} v_a(\mathbf{X}_i) \quad \text{as } \varphi_{0i} = (\sqrt{N})^{-1} \forall i, \end{aligned} \quad (\text{B4})$$

where we have switched to index notation for clarity. Thus, this term would not contribute to the flux under

the small gradients approximation. Similarly, the contribution from the term with the traveling wave velocity \mathbf{v}_w can be determined by plugging the adiabatic expression of σ_j as follows

$$\begin{aligned}
\mathcal{I}_w &\equiv Dv_w\tau \sum_{j=0}^{N-1} \varphi_{0j} \int_{h \neq 0} d\mathcal{X}_h v_a(\mathbf{X}_j - \mathbf{v}_w t) \partial_{0\beta} \delta_{\beta,w} \sigma_{j\alpha}, \\
&= -\frac{\tau^2 Dv_w}{d} \sum_{j=0}^{N-1} \varphi_{0j} \int_{h \neq 0} d\mathcal{X}_h v_a(\mathbf{X}_j - \mathbf{v}_w t) \times \\
&\quad \left[\sum_{l \neq 0} \varphi_{lj} \partial_{0\beta} \delta_{\beta,w} \partial_{l\alpha} [v_a(\mathbf{X}_j - \mathbf{v}_w t) \varrho] \right. \\
&\quad \left. - d \partial_{0\beta} \delta_{\beta,w} \partial_{i\beta} \gamma_i \chi_{i\beta} \sigma_{j\alpha} \right] + \mathcal{O}(\partial_{0\alpha}^2), \\
&= \frac{\tau^2 Dv_w}{d} \sum_{j=0}^{N-1} \varphi_{0j} \int_{h \neq 0} d\mathcal{X}_h [\partial_{l\alpha} v_a(\mathbf{X}_j - \mathbf{v}_w t)] \times \\
&\quad \varphi_{li} \partial_{0\beta} \delta_{\beta,w} [v_a(\mathbf{X}_i - \mathbf{v}_w t) \varrho] + \tau \gamma_j \mathcal{I}_w + \mathcal{O}(\partial_{0\alpha}^2), \\
&= \frac{\tau^2 Dv_w}{d} \sum_{j=0}^{N-1} \varphi_{0j} \int_{h \neq 0} d\mathcal{X}_h [\partial_{0\alpha} v_a(\mathbf{X}_j - \mathbf{v}_w t)] \times \\
&\quad \sqrt{N} \varphi_{li}^2 \partial_{0\beta} \delta_{\beta,w} [v_a(\mathbf{X}_i - \mathbf{v}_w t) \varrho] + \tau \gamma_j \mathcal{I}_w + \mathcal{O}(\partial_{0\alpha}^2), \tag{B5}
\end{aligned}$$

where we have used integration by parts to go from the second step to the third, and the identity Eq. (B4) in the final step. This implies,

$$\mathcal{I}_w (1 - \tau \gamma_j) = \mathcal{O}(\partial_{0\alpha}^2), \tag{B6}$$

i.e., the contribution \mathcal{I}_w is also at least second order in gradients $\mathcal{O}(\nabla_0^2)$.

Next, we consider the term with the activity

$$\begin{aligned}
&-\frac{\tau}{d} \sum_{j=0}^{N-1} \varphi_{0j} \int_{h \neq 0} d\mathcal{X}_h v_a \sum_{l=0}^{N-1} \nabla_l \cdot [\varphi_{lj} v_a \varrho], \\
&= -\frac{\tau}{d} \sum_{j=0}^{N-1} \varphi_{0j} \int_{h \neq 0} d\mathcal{X}_h v_a \partial_{0\alpha} [\varphi_{0i} v_a \varrho] \\
&\quad -\frac{\tau}{d} \sum_{j=0}^{N-1} \varphi_{0j} \sum_{l \neq 0} \int_{h \neq 0} d\mathcal{X}_h v_a \partial_{l\alpha} [\varphi_{lj} v_a \varrho], \\
&= -\frac{\tau}{d} \sum_{j=0}^{N-1} \varphi_{0j} \int_{h \neq 0} d\mathcal{X}_h [\varrho v_a \partial_{0\alpha} v_a + v_a^2 \partial_{0\alpha} \varrho] \\
&\quad + \frac{\tau}{d} \sum_{j=0}^{N-1} \varphi_{0j} \int_{h \neq 0} d\mathcal{X}_h \varrho \varphi_{ij}^2 \sqrt{N} v_a \partial_{0\alpha} v_a, \\
&= -\frac{(N-2)\tau}{2d} \rho_0 \partial_{0\alpha} v_a^2 \left(\frac{\mathbf{X}_0}{\sqrt{N}} \right) - \frac{\tau}{d} v_a^2 \left(\frac{\mathbf{X}_0}{\sqrt{N}} \right) \partial_{0\alpha} \rho_0 + \mathcal{O}(\partial_{0\alpha}^2), \tag{B7}
\end{aligned}$$

where, we have again used integration by parts to go from the second step to the third, and Eq. (B4). We have also made use of the properties of the orthogonalizing matrix

$\sum_{j=0}^{N-1} \sum_{l \neq 0} \varphi_{lj}^2 = \sum_{l \neq 0} l \neq 0 \delta_{ll} = N-1$. Furthermore, we have Taylor-expanded the quantity $\partial_{0\alpha} v_a^2(\mathbf{X}_i)$ as

$$\partial_{0\alpha} v_a^2(\mathbf{X}_i) = \partial_{0\alpha} v_a^2 \left(\sum_{j=0}^{N-1} \varphi_{ji} \chi_j \right) = \partial_{0\alpha} v_a^2(\varphi_{0i} \chi_0) + \mathcal{O}(\partial_{0\alpha}^2). \tag{B8}$$

Finally, we use the adiabatic expression of σ_j again to evaluate the contributions coming from the remaining term, which we define as $\sum_{i=0}^{N-1} \mathcal{I}_{i\alpha}$ with

$$\begin{aligned}
\mathcal{I}_{i\alpha} &\equiv -\tau \varphi_{0j} \int_{h \neq 0} d\mathcal{X}_h [\partial_{i\beta} v_a] \gamma_i \chi_{i\beta} \sigma_{j\alpha}, \\
&= \frac{\tau^2}{d} \varphi_{0j} \int_{h \neq 0} d\mathcal{X}_h [\partial_{i\beta} v_a] \gamma_i \chi_{i\beta} \partial_{l\alpha} [\varphi_{lj} v_a \varrho] \\
&\quad - \tau^2 \varphi_{0j} \int_{h \neq 0} d\mathcal{X}_h [\partial_{i\beta} v_a] \gamma_i \chi_{i\beta} \partial_{l\gamma} [\gamma_l \chi_{l\gamma} \sigma_{j\alpha}] + \mathcal{O}(\partial_{0\alpha}^2), \\
&= -\frac{\tau^2}{d} \varphi_{0j} \int_{h \neq 0} d\mathcal{X}_h [\partial_{i\beta} v_a] \gamma_i [\partial_{l\alpha} \chi_{i\beta}] \varphi_{lj} v_a \varrho \\
&\quad + \tau^2 \varphi_{0j} \int_{h \neq 0} d\mathcal{X}_h [\partial_{i\beta} v_a] \gamma_i [\partial_{l\gamma} \chi_{i\beta}] \gamma_l \chi_{l\gamma} \sigma_{j\alpha} + \mathcal{O}(\partial_{0\alpha}^2), \\
&= -\frac{\tau^2}{d} \varphi_{0j} \int_{h \neq 0} d\mathcal{X}_h [\partial_{i\beta} v_a] \gamma_i \varphi_{ij} v_a \varrho - \tau \gamma_i \mathcal{I}_{i\alpha} + \mathcal{O}(\partial_{0\alpha}^2), \\
&= -\frac{\tau^2}{d} \varphi_{0j} \int_{h \neq 0} d\mathcal{X}_h \sqrt{N} \varphi_{ij}^2 \gamma_i \varrho v_a [\partial_{0\alpha} v_a] - \tau \gamma_i \mathcal{I}_{i\alpha} + \mathcal{O}(\partial_{0\alpha}^2), \\
&= -\frac{\tau^2}{2d} \gamma_i \rho_0 \partial_{0\alpha} v_a \left(\frac{\mathbf{X}_0}{\sqrt{N}} \right) - \tau \gamma_i \mathcal{I}_{i\alpha} + \mathcal{O}(\partial_{0\alpha}^2), \tag{B9}
\end{aligned}$$

where, we have used integration by parts in the first line and in going from second to the third step. We have also used the identity Eq. (B4) and the Taylor expansion Eq. (B8) in the penultimate step. Solving the resulting linear equation for $\mathcal{I}_{i\alpha}$, we get

$$\sum_{i=0}^{N-1} \mathcal{I}_{i\alpha} = -\frac{\tau}{2d} [N-2+\epsilon] \rho_0 \partial_{0\alpha} v_a \left(\frac{\mathbf{X}_0}{\sqrt{N}} \right) + \mathcal{O}(\partial_{0\alpha}^2), \tag{B10}$$

where ϵ is the tactic response parameter defined in the main text in Eq. (11). Putting everything together from Eqs. (B3)- (B10) in the probability current for ρ_0 , we have

$$\mathcal{J} = -\frac{\tau\epsilon}{2d} \rho_0 \nabla_0 v_a^2 \left(\frac{\mathbf{X}_0}{\sqrt{N}} \right) - \left[D + \frac{\tau}{d} v_a^2 \left(\frac{\mathbf{X}_0}{\sqrt{N}} \right) \right] \nabla_0 \rho_0 - \mathbf{v}_w \rho_0 + \mathcal{O}(\nabla_0^2). \tag{B11}$$

Finally, we apply the chain rule to write the drift-diffusion equation Eq. (9) with the effect drift and diffusivity defined in Eq. (10).

Appendix C: Steady State Density Profile in Co-moving Frame

Here, we sketch the derivation to obtain the steady state density profile with a constant flux J (Eq. (12))

in a co-moving box of length L endowed with periodic boundary conditions. We derive everything in one dimension for simplicity, however, it can be easily generalized to higher dimensions. We start with the continuity equation,

$$\partial_x \rho(x) + b(x)\rho(x) = -D^{-1}(x)J, \quad (\text{C1})$$

where we defined the function $b(x) = -V(x)/D(x)$ for brevity. Solving this equation with the integrating factor

$$\begin{aligned} \partial_x \left[\rho(x) \exp \left\{ \int_0^x dx' b(x') \right\} \right] = \\ - JD^{-1}(x) \exp \left\{ \int_0^x dx' b(x') \right\}. \end{aligned} \quad (\text{C2})$$

Integrating this equation over a box length (y to $y+L$) and using the periodic boundary conditions, i.e., $\rho(y+L) = \rho(y)$, we have

$$\begin{aligned} \rho(y) \exp \left[\int_0^y dx' b(x') \right] \left\{ \exp \left[\int_y^{y+L} dx' b(x') \right] - 1 \right\} \\ = -J \int_y^{y+L} dx D^{-1}(x) \exp \left\{ \int_0^x dx' b(x') \right\}. \end{aligned} \quad (\text{C3})$$

Since $D^{-1}(x)$ and $b(x)$ is also periodic, we have $\exp \left\{ \int_y^{y+L} dx b(x) \right\} = \exp \left\{ \int_0^L dx b(x) \right\}$. Rearranging some terms, we arrive at

$$\begin{aligned} \rho(y) \left\{ 1 - \exp \left[\int_0^L dx' b(x') \right] \right\} \\ = JD^{-1}(y) \int_y^{y+L} dx \exp \left\{ \int_y^x dx' b(x') \right\}. \end{aligned} \quad (\text{C4})$$

Finally, using $\int_0^L dy \rho(y) = \rho_b L$, we have

$$J = \frac{\rho_b L \left\{ 1 - \exp \left[\int_0^L dx' b(x') \right] \right\}}{\int_0^L dy D^{-1}(y) \int_0^L dx \exp \left[\int_y^{y+x} dx' b(x') \right]}. \quad (\text{C5})$$

Plugging this expression for J in Eq. (C4), we get the expression for the steady state density profile

$$\frac{\rho(y)}{\rho_b} = \frac{LD^{-1}(y) \int_0^L dx \exp \left\{ \int_y^{y+x} dx' b(x') \right\}}{\int_0^L dy D^{-1}(y) \int_0^L dx \exp \left\{ \int_y^{y+x} dx' b(x') \right\}}. \quad (\text{C6})$$

Appendix D: Simulation Details

All numerical data has been generated using Langevin dynamics simulations of the monomer equations of motion in Eq. (2) and their orientations in Eq. (3). These equations are discretized using the standard Euler-Maruyama scheme and read

$$\begin{aligned} \mathbf{X}_i(t + \Delta t) = \mathbf{X}_i(t) + \sqrt{2\Delta t D} \boldsymbol{\xi}_i(t) \\ + \mu \Delta t \left[- \sum_{j=0}^{N-1} M_{ij} \mathbf{X}_j(t) + v_a (\mathbf{X}_i(t) - \mathbf{v}_w t) \boldsymbol{\eta}_i(t) \right], \\ \boldsymbol{\eta}_i(t + \Delta t) = \boldsymbol{\eta}_i(t) - \tau^{-1} \Delta t \boldsymbol{\eta}_i(t) + \sqrt{2\Delta t (\tau d)^{-1}} \boldsymbol{\zeta}_i(t), \end{aligned} \quad (\text{D1})$$

where Δt is the discretization timestep, and was chosen as $\Delta t = 0.01$ for all simulations. $\boldsymbol{\xi}_i(t)$ and $\boldsymbol{\zeta}_i(t)$ are independent Gaussian random variables with zero mean and unit variance. All simulations have been performed in a box of size $L = 10$ with periodic boundary conditions. The steady state density profiles in Fig. 2 and Fig. 3 were obtained using time-averaging from a single simulation of 10^9 simulation steps. For Fig. 4 and Fig. 5, the drift of the center of mass was measured for 10^3 independent trajectories, each 10^6 timesteps long. The numerical errors are within the size of the symbols in all figures.